Journal of Zhejiang University-SCIENCE A 2025 26(10):917-930
www.jzus.zju.edu.cn; www.springer.com/journal/11582
E-mail: jzus_a@zju.edu.cn

Research Article

https://doi.org/10.1631/jzus.A2400437

Check for updates

Manufacturing and thermal properties of steel–carbon fibre/polyetheretherketone (CF/PEEK) hybrid shafts using laser-assisted in-situ consolidation

Zequan DING[1,2], Congcong LUAN[1,2,3]✉, Xinhua YAO[1,2], Lingyu CHENG[4], Yuyang JI[1,2], Chengcheng NIU[1,2], Ningguo DONG[1,2], Kai ZHAO[4], Zhibin RUAN[5], Jianzhong FU[1,2]

[1]*State Key Laboratory of Fluid Power and Mechatronic Systems, College of Mechanical Engineering, Zhejiang University, Hangzhou 310058, China*
[2]*Key Laboratory of 3D Printing Process and Equipment of Zhejiang Province, College of Mechanical Engineering, Zhejiang University, Hangzhou 310058, China*
[3]*State Key Laboratory of Mechanical Transmission for Advanced Equipment, Chongqing University, Chongqing 400044, China*
[4]*Shanghai Aerospace Equipment Manufacturing Co. Ltd., Shanghai 200245, China*
[5]*Zhejiang Advanced CNC Machine Tool Technology Innovation Center Co., Ltd., Taizhou 317500, China*

Abstract: A novel steel–carbon fibre/polyetheretherketone (CF/PEEK) hybrid shaft is proposed, considering the thermal stability, negative coefficient of thermal expansion in fibre orientation, and high stiffness of CF/PEEK, which is expected to suppress the thermal deformation of shafts. A laser-assisted in-situ consolidation (LAC) process, together with its equipment, was developed to manufacture the hybrid shaft. Firstly, the optimal process parameters, including the laser-heated temperature and placement speed, were investigated. A maximum short-beam shear strength of 80.7 MPa was achieved when the laser-heated temperature was 500 °C and the placement speed was 100 mm/s. In addition, the failure modes and the effect of environmental temperature on the CF/PEEK samples were analyzed. Both interlayer cracks and inelastic deformation failure modes were observed. The formation and propagation of cracks were further investigated through digital image correlation (DIC). Furthermore, internal defects of the CF/PEEK sample were detected using X-ray tomography scans, and a minimum porosity of 0.23% was achieved with the optimal process parameters. Finally, two steel–CF/PEEK hybrid shafts, with different fibre orientations, were manufactured based on the optimal process parameters. The surface temperature distributions and thermal deformations were investigated using a self-established deformation/temperature measurement platform. The hybrid shaft showed an 85.7% reduction in radial displacement with hoop fibre orientation and an 11.5% reduction in axial displacement with cross fibre orientation compared with the steel shaft. The results indicate that the proposed method has great potential to improve the thermal stability of hybrid shafts and the accuracy of machine tools.

Key words: Thermal characteristics; Steel–carbon fibre/polyetheretherketone (CF/PEEK) hybrid shaft; Laser-assisted in-situ consolidation (LAC); Thermal deformation

1 Introduction

The thermal characteristics of shafts have a significant impact on the accuracy and stability of rotary machines, especially precision machine tools. About 40%–70% of the total manufacturing error is caused by the thermal deformation of the shaft in precision machine tools (Mayr et al., 2012). Passive cooling (Fan et al., 2022; Lei et al., 2022; Zheng and Chen, 2022; Li MY et al., 2023a; Li ZL et al., 2023), thermal structure optimization design (Xia et al., 2015; Li MY et al., 2023a, 2023b; Li Y et al., 2023b; Li ZL et al., 2023), and thermal error compensation (Bao et al., 2023; Li Y et al., 2023a; Lu et al., 2023; Song et al., 2023) are the three main measures used to improve machining accuracy. Thermal structure optimization design is expected to reduce the thermal deformation from the origin, without an external cooling system or

✉ Congcong LUAN, lccshdg@zju.edu.cn
Zequan DING, https://orcid.org/0009-0005-9287-1325
Congcong LUAN, https://orcid.org/0000-0001-6289-9400

Received Sept. 4, 2024; Revision accepted Dec. 20, 2024;
Crosschecked Aug. 3, 2025; Online first Sept. 18, 2025

sensors. New materials, including ceramics and carbon fibre (CF), have been introduced during the optimization of thermal structure design, considering their thermal stability (Vermeulen et al., 2000; Namba, 2001; Ding et al., 2016; Xu et al., 2016; Ge and Ding, 2018).

Polyetheretherketone (PEEK), as a high-performance thermoplastic, is widely applied as the matrix for CF reinforced composites in mechanical, aerospace, and other fields due to its excellent mechanical properties, high thermostability, corrosion resistance, and shock absorption (Moddeman et al., 1986; Cebe et al., 1987; Cirino et al., 1987; Grove, 1993; Pratte, 2012; Ji et al., 2015; Guo et al., 2024). Furthermore, CF has a negative coefficient of thermal expansion in the fibre direction, which is thought to compensate for thermal deformation. Thus, carbon fibre reinforced polyetheretherketone (CF/PEEK) is considered a great candidate to improve the thermal characteristics of shafts. However, how best to combine CF/PEEK with steel to produce a hybrid shaft needs investigation, and the high melting point (exceeding 340 °C) and viscosity of PEEK create great challenges to the intimate interface bonding required during the manufacture of steel–CF/PEEK hybrid shafts (Levy et al., 2014; Stokes-Griffin and Compston, 2016; Çelik et al., 2020, 2021).

Fortunately, rapid heating can be achieved by laser and a high-temperature area of up to 600 °C can be acquired within several hundred milliseconds (Stokes-Griffin and Compston, 2015). This can be used as the heating source during the in-situ consolidation process called laser-assisted in-situ consolidation (LAC). The mechanism and behavior of laser irradiation on CF/PEEK prepreg during the LAC process have been investigated in our previous work (Ji et al., 2023). The effects of process parameters, including laser power and placement speed, on the crystallinity and mechanical properties were analyzed in detail. In addition, the effect of the shadow region on the heating temperature distribution was revealed (Jiang et al., 2023). Furthermore, the combined effects of laser power, placement speed, and consolidation force on the shear strength were investigated, and a maximum shear strength of 78 MPa was achieved (Comer et al., 2015; Miao et al., 2021). Therefore, the LAC process is expected to realize the intimate interface bonding of steel–CF/PEEK hybrid shafts, although it has never been applied to the manufacture of large curvature structures. Besides, the thermal characteristics, such as thermal deformation and surface temperature distribution of steel–CF/PEEK hybrid shafts manufactured by the LAC process, still need to be investigated and analyzed.

This study aimed to explore the feasibility of steel–CF/PEEK hybrid shafts manufactured by the LAC process. The principle and platform of the hybrid shaft manufacturing process were established. The optimal process parameters were obtained through a series of short-beam shear (SBS) strength tests. In addition, failure modes and internal defects were analyzed using digital image correlation (DIC) and X-ray tomography scans. Finally, steel–CF/PEEK hybrid shafts with different fibre orientations were designed and manufactured. Meanwhile, the thermal characteristics of different steel–CF/PEEK hybrid shafts were investigated by comparing them with a steel shaft using a self-developed deformation/temperature measurement platform.

2 Materials and experiments

2.1 Principle and platform of hybrid shaft manufacturing

The principle of hybrid shaft manufacturing using the LAC process is shown in Fig. 1a. The CF/PEEK prepreg is placed on the steel core shaft under the

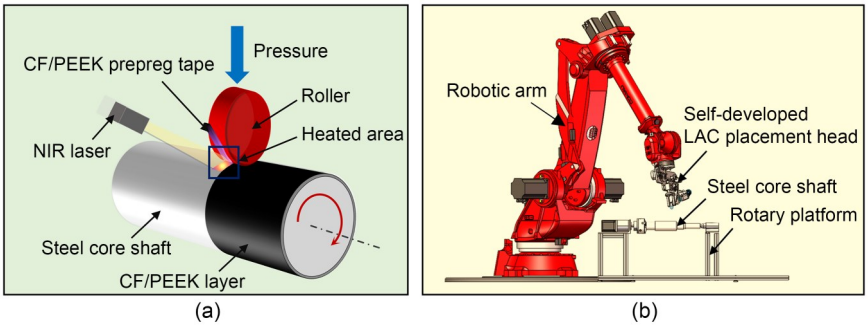

Fig. 1 Hybrid shaft manufacturing with the LAC process: (a) principle of LAC; (b) manufacturing platform

heating of a near-infrared (NIR) laser and pressure provided by the roller. The main principle is that the laser simultaneously irradiates the CF/PEEK prepreg tape and CF/PEEK layer that has already been placed on the steel core shaft, melting the PEEK resin on both surfaces of the CF/PEEK layer and CF/PEEK prepreg tape. Meanwhile, a rubber roller is used to press incoming CF/PEEK prepreg tape on the CF/PEEK layer. Under a consolidation force, the melted areas contact each other at the nip point, and new molecular chains form between the melted resins, achieving high-strength additive manufacturing of CF/PEEK prepreg tape.

A self-developed LAC process platform based on the above principle was established, including a self-developed LAC placement head, assembled at the end of the sixth axis of the robotic arm NJ220-2.7 (COMAU, Italy), and a rotary platform, collaboratively controlled by robotic system (Fig. 1b). The steel core shaft is clamped on the rotary platform through a three-jaw chuck, rotating along with the motor. The fibre orientation can be adjusted by controlling the angle between the roller axis and the core shaft axis through the rotation of the robotic arm. The outside surface linear velocity of the core shaft and the roller movement speed along the axis of the core shaft can be obtained based on the optimal placement speed and the angle between the axes of the roller and the core shaft, according to the speed decomposition law.

2.2 Materials

In this study, we used T800 CF/PEEK prepreg tape (HENGBO, China) containing 34% mass fraction PEEK. The prepreg tape was 6.35 mm wide and 0.21 mm thick. S45C steel, a medium carbon structural steel, was adopted as the core shaft, considering its compatibility with other machine tool components and overall comprehensive performance. The thermal and mechanical properties of the CF/PEEK and S45C steel are listed in Table 1.

3 Results and discussion

3.1 Optimization of LAC process

3.1.1 SBS and DIC test

SBS tests were conducted to investigate the optimal parameters of the LAC process, and DIC MatchID-Stereo HR (MatchID, Belgium) was applied simultaneously to illustrate the failure mode of samples during SBS tests. The experimental equipment and process are shown in Fig. 2. An electronic universal testing machine UTM5105 (Suns, China), fitted with a high/low temperature chamber, was adopted to conduct SBS tests under different ambient temperatures. A customized fixture was used to satisfy the testing condition according to ASTM D2344 (ASTM, 2024) (Fig. 2b). The loading speed was set at 1 mm/min. Meanwhile, DIC equipment, including two cameras and two light-emitting diode (LED) light sources, was positioned in front of the SBS testing area (Fig. 2a). The focal length and depth of field of both cameras were adjusted to ensure that the painting area on the samples was in the same position in the captured images. Before the experiment, a dedicated calibration plate was placed in front of the sample manually and slightly changed its spatial position and tilt angle, while 20 pictures were captured by cameras to calculate the distance between two points in the photos and iterate various algorithms in the software to obtain the best signal-to-noise ratio for sample strain calculation. Subsequently, during SBS tests, the loading process was recorded by cameras, with a sampling frequency of 1 Hz.

A series of CF/PEEK specimens were manufactured at different laser-heated temperatures and placement speeds. The total number of CF/PEEK prepreg tape layers was set to 16, resulting in a series of layers at least 2.4 mm thick. The robotic arm automatically lifted 0.15 mm for manufacturing each ply according to the program to ensure that the laser irradiation position and angle did not deviate. After completing the

Table 1 Thermal and mechanical properties of T800 CF/PEEK prepreg tape and S45C steel

Item	Specific heat capacity (J/(kg·K))	Thermal conductivity (W/(m·K))	Emissivity	Coefficient of thermal expansion (K^{-1})	Elastic modulus (GPa)	Shear modulus (GPa)
S45C steel	460	50	0.13	11.6×10^{-6}	210.0	80
CF/PEEK (longitudinal)	1600	160	0.71	-0.09×10^{-6}	243.3	–
CF/PEEK (transverse)	1600	0.64	0.71	22.4×10^{-6}	8.0	–

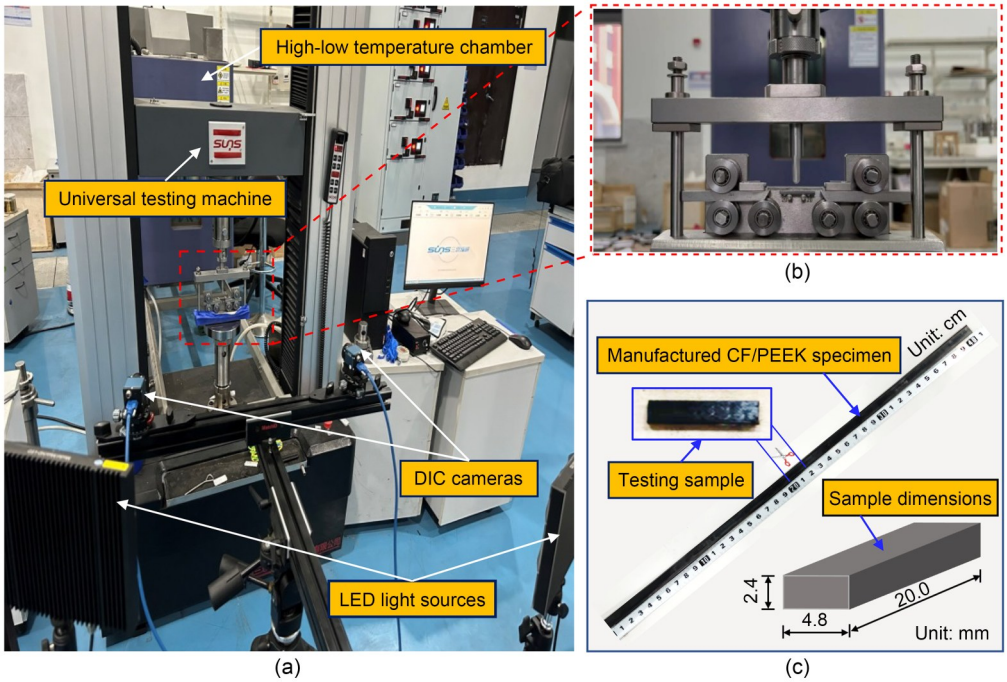

Fig. 2 Short beam strengths and DIC tests: (a) overall testing equipment; (b) customized fixture; (c) prepared sample and sample dimensions

manufacture of the CF/PEEK prepreg tape, the formed CF/PEEK naturally cooled to room temperature before proceeding with the incoming CF/PEEK prepreg tape. Specific manufacturing process parameters are listed in Table 2, which were determined according to the physical properties of CF/PEEK, reported literature, and our pre-experiments (Donough et al., 2022; Ji et al., 2023; Niu et al., 2024).

Table 2 Manufacturing process parameters in SBS tests

Process parameter	Value
Laser-heated temperature (°C)	400, 450, 500, 550
Placement speed (mm/s)	25, 50, 75, 100
Consolidation pressure (MPa)	0.6
Irradiation angle (°)	24

After manufacturing all CF/PEEK specimens, five samples were prepared for each specimen. The final cross-sectional size of each sample was 2.4 mm× 4.8 mm. The prepared specimens and the dimensions of the samples are shown in Fig. 2c. Considering the acceleration of the robotic arm movement and the time required for the rollers to reach a stable working temperature, samples were taken at a distance of 200 mm from the starting point to ensure that the performance of samples truly reflected the bonding quality under different process parameters. The SBS strength of each sample was calculated using the following equation:

$$\sigma_{SBS}=0.75\times F_{max}/(b\times h), \quad (1)$$

where F_{max} is the maximum force recorded in the SBS test, b is the width, and h is the thickness of the sample. For the DIC tests, each sample was subjected to spray painting treatment, and small spots were observed on the surface for calculating strain and displacement.

The effect of ambient temperature on the SBS of CF/PEEK was also investigated. Considering the working conditions of the shaft, tests at four ambient temperatures, 40, 50, 60, and 70 °C, with 60% humidity, were conducted in a high-low temperature chamber. After the samples were put in, it took 20 min for the temperature inside the chamber to reach the set value before starting the SBS test.

3.1.2 Result of SBS

The influence of laser-heated temperature and placement speed on CF/PEEK SBS is shown in Fig. 3. For the four placement speeds used in the experiment, SBS strength exhibited two different trends of change. When the process temperature was 400 or 450 °C, the SBS strength gradually decreased with increasing

placement speed. On the other hand, when the process temperature exceeded 500 ℃, as the placement speed increased, the SBS strength first decreased and then increased. The highest SBS strength of 80.7 MPa was obtained with a 500 ℃ process temperature and 100 mm/s placement speed.

3.1.3 Failure modes

To further evaluate the manufacturing quality of samples, the failure modes in SBS tests were investigated and analyzed. Both interlayer cracks and inelastic deformation failure modes were observed (Fig. 4). The failure modes were closely related to the load-bearing capabilities, and interlayer cracks appeared on the surface of samples when the SBS strength was less than 65 MPa (Fig. 4a). Samples suffered inelastic deformation instead of cracking when the SBS strength was greater than 65 MPa (Fig. 4b).

Furthermore, the formation and propagation of cracks were investigated by DIC. The maximum principal strain of the sample during the SBS test was observed (Fig. 5). When the load reached a critical value, a large principal strain first appeared in an interface near the loading head directly below the force point, indicating the generation of a crack (Fig. 5a). Under the action of the loading head, the sample underwent bending, and different layers of CF/PEEK were subjected to different principal stresses. Since the interface bonding quality was relatively weak, it was prone to producing large strains at interfaces due to the lack of CFs providing greater stiffness. Thus, the undamaged interlayer area exhibited greater strain than adjacent areas. As the load increased further, the principal strain located at the same interface gradually increased and extended towards the end face of the sample (Fig. 5b). After 300 s loading, a new large principal

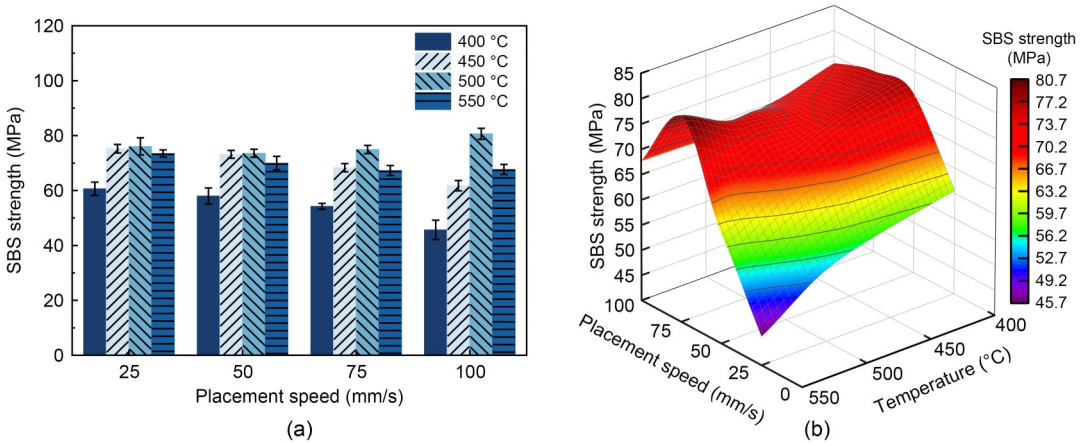

Fig. 3 SBS results: (a) SBS strength with different laser-heated temperatures and placement speeds; (b) synthetic influence surface showing the effect of laser-heated temperature and placement speed on interlaminar shear strength

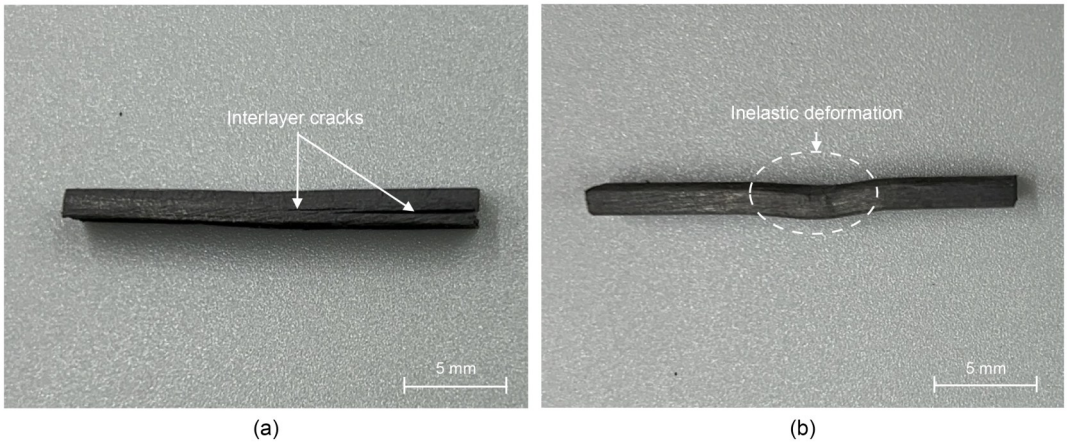

Fig. 4 Two failure modes in SBS tests: (a) interlayer cracks; (b) inelastic deformation

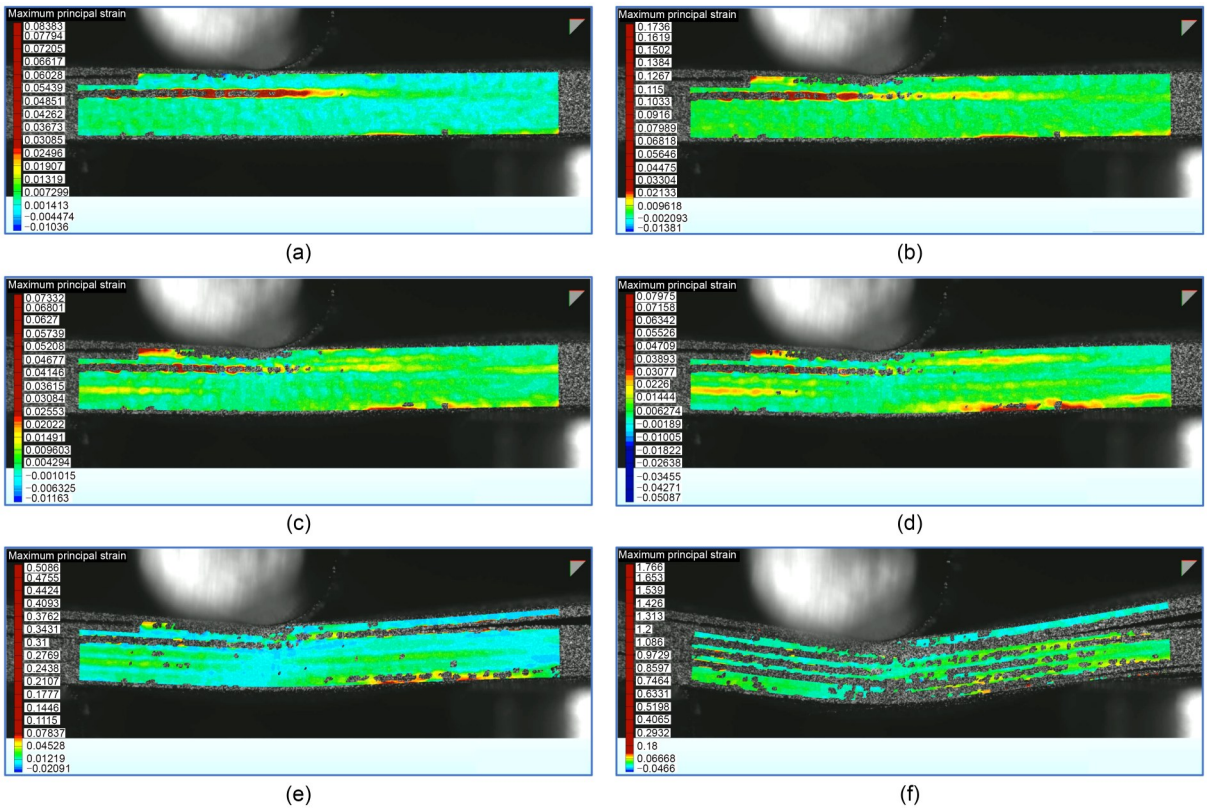

Fig. 5 Crack formation and propagation of samples revealed by DIC: (a) loading time at 168 s; (b) loading time at 240 s; (c) loading time at 300 s; (d) loading time at 352 s; (e) loading time at 416 s; (f) loading time at 688 s

strain area was observed on the left side below the loading area (Fig. 5c). Subsequently, for all cracking interlayers, the areas of the large principal strain were extended further along the interface. A new large principal strain interface appeared at the bottom of the sample and to the right of the loading area, indicating that a new crack had formed (Fig. 5d). After 416 s of loading, the newly formed crack rapidly propagated to the right end of the sample, forming a complete notch (Fig. 5e). The entire testing period finished after 688 s of loading. The final sample morphology, with multiple interlayer cracking failures, is shown in Fig. 5f. All cracks underwent a similar formation propagation process until the end of loading. The upper and lower surfaces of some cracks were refitted under increasing loads, especially in the area adjacent to the centre loading areas. All failure positions were equidistant and parallel to the fibre direction at the interlayer areas, indicating that interlayer strength has a significant impact on the load-bearing capacity of CF/PEEK structures.

Based on the location of one crack, the crack opening data of each point on the crack were extracted (Fig. 6). Before the crack appeared, each point on the

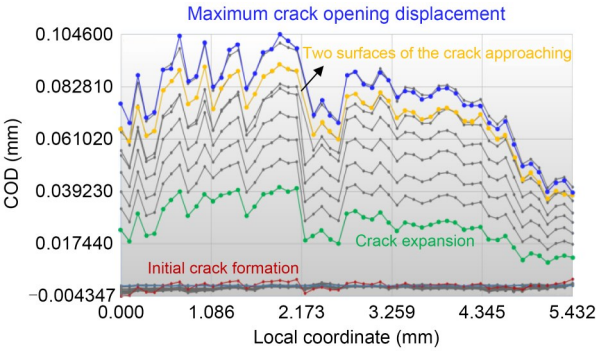

Fig. 6 Crack propagation of samples during SBS tests. COD is the crack opening distance. References to color refer to the online version of this figure

selected crack barely moved in the observed plane (red line). In the crack expansion stage, as the load increased, the distance between the upper and lower surfaces significantly increased at a certain moment, indicating the sudden formation of the crack (green line). The opening distance tended to decrease from one end to the centre of the sample. The propagation of cracks had a unified characteristic once the initial crack appeared. We attributed this to the high stiffness

of the CF/PEEK along the fibre direction, maintaining a relatively stable failure morphology on both sides of the fracture. The displacement of each point increased uniformly along the crack until the maximum displacement of 0.1046 mm was reached (blue line). At this stage, stress was released through the continuous expansion of cracks to withstand the gradually increasing pressure. After that, with a further increase in pressure force, the crack opening distance began to decrease. The upper and lower sides of the crack tended to contact again, and the sample continued to withstand external loads as an entire part. To further investigate the fracture behavior of CF/PEEK composites manufactured using the LAC process, the failure morphology of cracks was analyzed using a field emission scanning electronic microscope (FESEM, Zeiss G300, Germany) (Fig. 7). Debonding of the interface between the CFs and the PEEK matrix was observed accompanying the cracking of the PEEK matrix, indicating that a good interlayer bonding quality was achieved. However, the interface between the CFs and the PEEK matrix needs further improvement.

3.1.4 Internal defects

To further characterize the performance of interface bonding, the internal defects of two samples, manufactured at 400 °C, 75 mm/s and 500 °C, 100 mm/s, respectively, were detected through 3D X-ray tomography scans (Xradia 515 Versa, Zeiss, Germany). The voxel size was set at 1 μm^3 during 3D X-ray scanning. CFs, PEEK, and voids could be clearly distinguished due to their different optical properties, and the obtained data were used for 3D reconstruction to generate a 3D structure of the local area. A total of 1000 slices were obtained for 3D reconstruction of the whole scanning region. The porosity of the detected area of the CF/PEEK sample was calculated using Dragonfly Pro analysis software.

For the sample manufactured with 400 °C and 75 mm/s process parameters, five interlayers, formed by the enrichment of PEEK, and the interior of the CF prepreg can be observed (Fig. 8). A porosity of 0.23% was achieved for the CF/PEEK component, and a void enrichment area was observed at interlayer-iii, with a maximum void width of 8.9 μm. Further observation of interlayer-iii revealed a series of defects arranged along the CFs near this void, as well as a fibre with an inconsistent arrangement direction. This may have been due to fluctuations in the surface quality and PEEK content. However, voids deteriorate the performance of CF/PEEK structural components and can become the source of cracking failure.

A cross-section view of the sample, manufactured with the optimal process parameters, is shown in Fig. 8b. There is no obvious interlayer area. All CFs are evenly distributed throughout the entire observation field, indicating that the load-bearing capacity of the entire section is uniform and the load-bearing capacity of the sample is enhanced. Therefore, the inelastic deformation failure mode is inclined to appear. The porosity was also calculated. Only 0.01% volume of voids was detected, proving that the quality of the entire CF/PEEK sample, manufactured with optimal parameters, is reliable.

3.1.5 Effect of ambient temperature on SBS

To investigate the effect of ambient temperature on the performance of CF/PEEK, the SBS of samples manufactured with the optimal parameters under different ambient temperatures was tested (Fig. 9). The

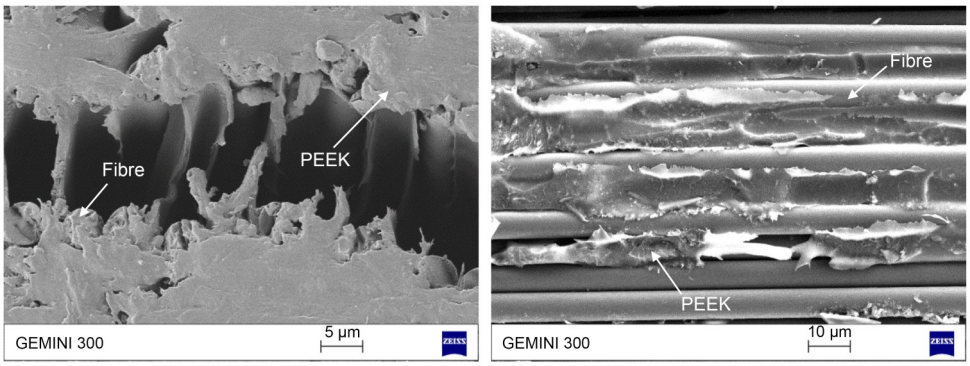

Fig. 7 Failure morphology of cracks: (a) cross section; (b) surface of a crack

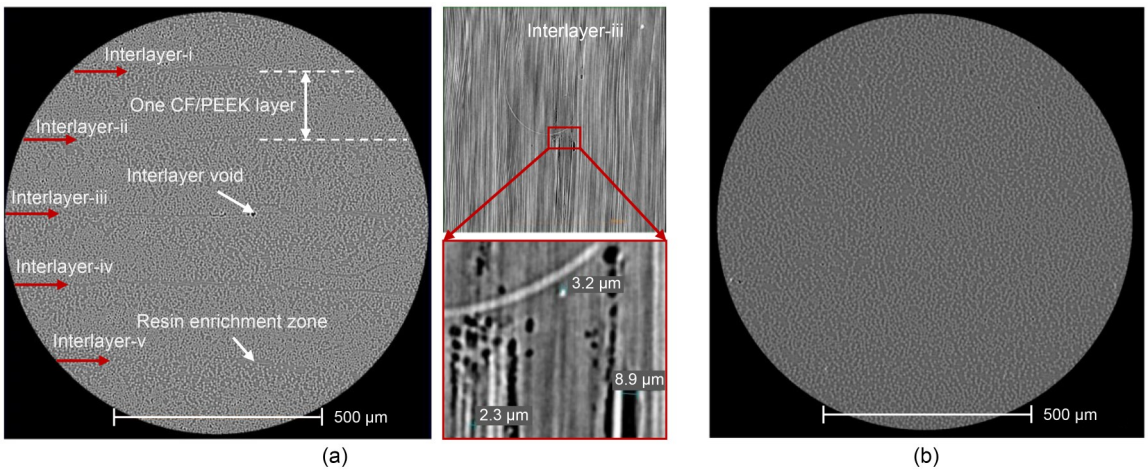

Fig. 8 X-ray tomography of CF/PEEK sample: (a) manufactured with 400 ℃ and 75 mm/s process parameters and the amplification of interlayer-iii; (b) manufactured with 500 ℃ and 100 mm/s process parameters

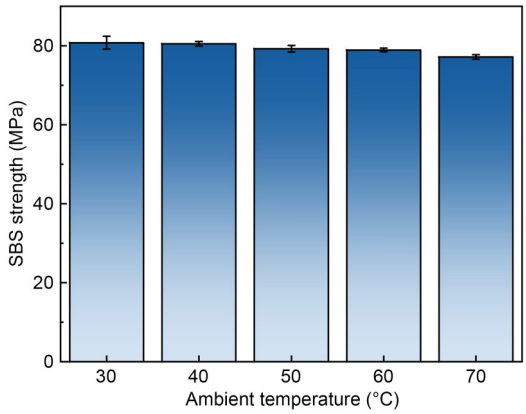

Fig. 9 Effect of ambient temperature on CF/PEEK SBS strength

SBS decreased slightly with increasing ambient temperature. There was about a 4.3% decline when the temperature rose to 70 ℃, compared with the highest SBS of the sample at 20 ℃. In addition, inelastic deformation failure was observed for all tested samples, indicating that the ambient temperature did not significantly affect the interlayer bonding quality. It also showed that CF/PEEK can be used in steel–CF/PEEK hybrid shafts, which usually operate below 70 ℃, because of its good thermal stability.

3.2 Manufacturing of steel–CF/PEEK hybrid shaft

To verify the effect of CF/PEEK on shaft thermal deformation, a 3-mm thick CF/PEEK part was introduced to replace a portion of S45C steel on the outside part of the steel core shaft in the middle area between the bearing areas I and II, with two fibre orientation arrangement methods, respectively (Fig. 10a). The two methods included a hoop-orientation arrangement and a cross-orientation arrangement. In the hoop-orientation arrangement, the CFs maintain consistent circumferential, namely at 90° to the centerline of the core shaft. In the cross-orientation arrangement, the CF/PEEK prepreg tapes are stacked in a ±45° sequence. The first layer of CF/PEEK for the two hybrid shafts was arranged in the cross-orientation. For the first steel–CF/PEEK hybrid shaft, all CF/PEEK prepreg tapes were arranged in the hoop-orientation, and for the second, they were arranged in the cross-orientation, except for the first layer. The specifications of the steel–CF/PEEK hybrid shaft are shown in Fig. 10b. For comparison, a steel shaft of the same size was made using S45C steel as a reference.

Steel–CF/PEEK hybrid shafts were manufactured using the self-developed manufacturing platform (Fig. 11a). The steel core shaft (Fig. 11b) was manufactured in advance using a traditional mechanical processing method. For further CF/PEEK manufacturing, the LAC process was applied, with the optimal combination of laser-heat temperature and placement speed. A robotic arm drove the LAC placement head to press CF/PEEK prepreg tape at the starting point of the path, and then the robotic arm and core shaft, both axes of which were adjusted to a certain angle, rotated at the set speed, in conjunction with the function of the laser, to complete the entire CF/PEEK manufacturing process. The manufacture of cross-orientation and hoop-orientation CF/PEEK is shown in Figs. 11c and 11d, respectively. Finally, steel–CF/PEEK hybrid shafts,

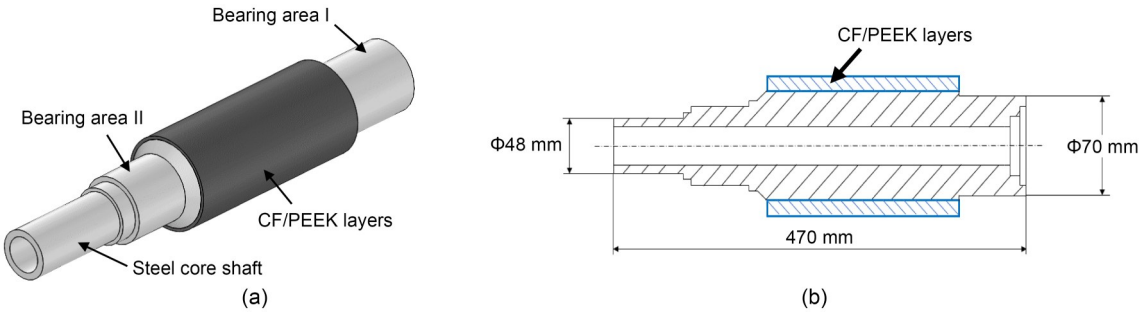

Fig. 10 Schematic diagram of a steel–CF/PEEK hybrid shaft: (a) CF/PEEK position on the shaft; (b) specific dimensions

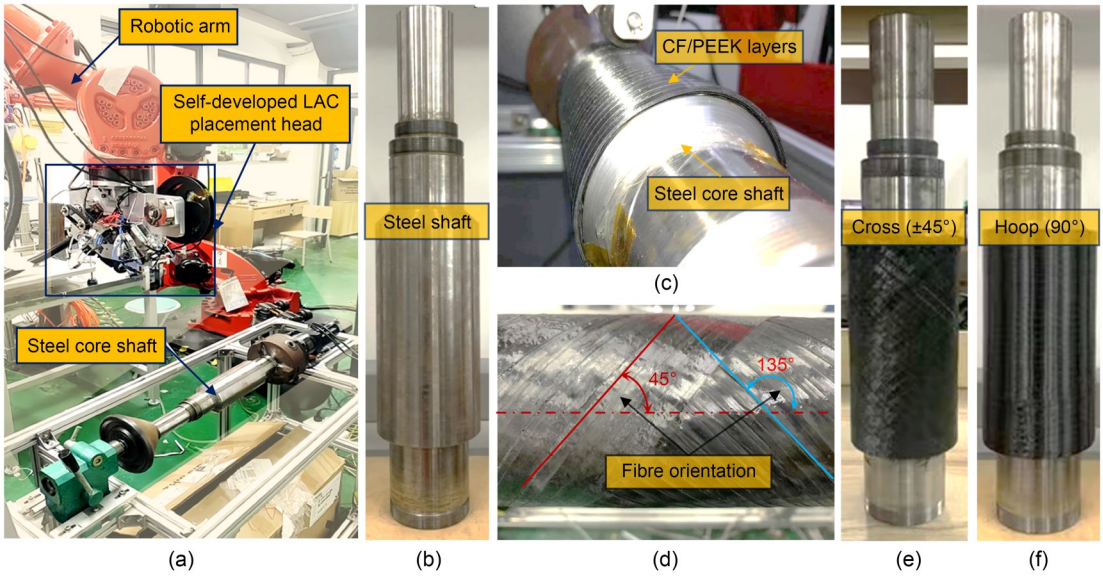

Fig. 11 Manufacture of steel–CF/PEEK hybrid shafts: (a) additive manufacturing platform before the manufacturing process; (b) steel core shaft; (c) manufacturing according to hoop-orientation; (d) manufacturing according to cross-orientation; (e) hybrid shaft with cross-orientation; (f) hybrid shaft with hoop-orientation

with cross-orientation and hoop-orientation, are shown in Figs. 11e and 11f, respectively.

3.3 Thermal properties of steel–CF/PEEK hybrid shafts

To evaluate the thermal characteristics of the two steel–CF/PEEK hybrid shafts and the steel shaft, a thermal deformation/temperature measurement platform was established to detect the axial thermal deformation and surface temperature of the shafts (Fig. 12). During the measurement process, shafts were placed on a flat insulation plate to minimize heat loss through thermal conduction. Shafts were heated using two silicone rubber heaters fixed on the outside surfaces of bearing areas I and II, simulating the frictional heat under actual working conditions. The heating temperature could be controlled within ±1 °C of the setting value. In this experiment, the heating areas were heated from 20 to 70 °C. Meanwhile, laser Doppler interferometers were used to measure the axial and radial thermal deformations once the two silicone rubber heaters operated. The laser emitted a single-frequency beam into a linear interferometer, which was then divided into two beams. One spectroscope was attached to the end of the shaft and another to the outer surface of the shaft between two bearing areas. The corresponding laser provided a vertical laser. The signal acquisition system calculated the amount of deformation according to the difference between the original beam and the spectroscope-reflected beam. Five temperature sensors, labelled T1 to T5, were arranged on the outside surfaces of the detecting shaft to measure the surface temperature, and two temperature sensors, labelled T6 and T7, were arranged on a steel frame

support to measure the environmental temperature changes of the workbench to eliminate errors. The measurement time was set to 8000 s, and the sampling frequency was 1 Hz.

The surface temperature distributions of two hybrid shafts and a steel shaft are shown in Figs. 13a–13c and a comparison of detection-point temperatures is shown in Fig. 13d. For detection points T1 and T2, an identical temperature distribution was observed for all three shafts, around 52 ℃ for T1 and 56.8 ℃ for T2. Due to the absence of CFs in this area, the temperature depends mainly on the specific heat capacity of the steel and the convective heat dissipation of the air. However, the temperature measured by T2 on the two

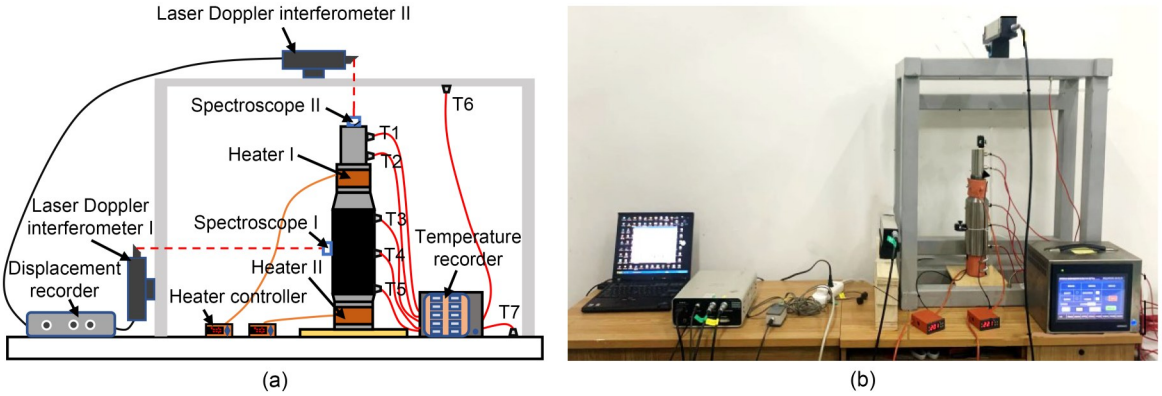

Fig. 12 Deformation/temperature measurement platform: (a) schematic image; (b) physical image

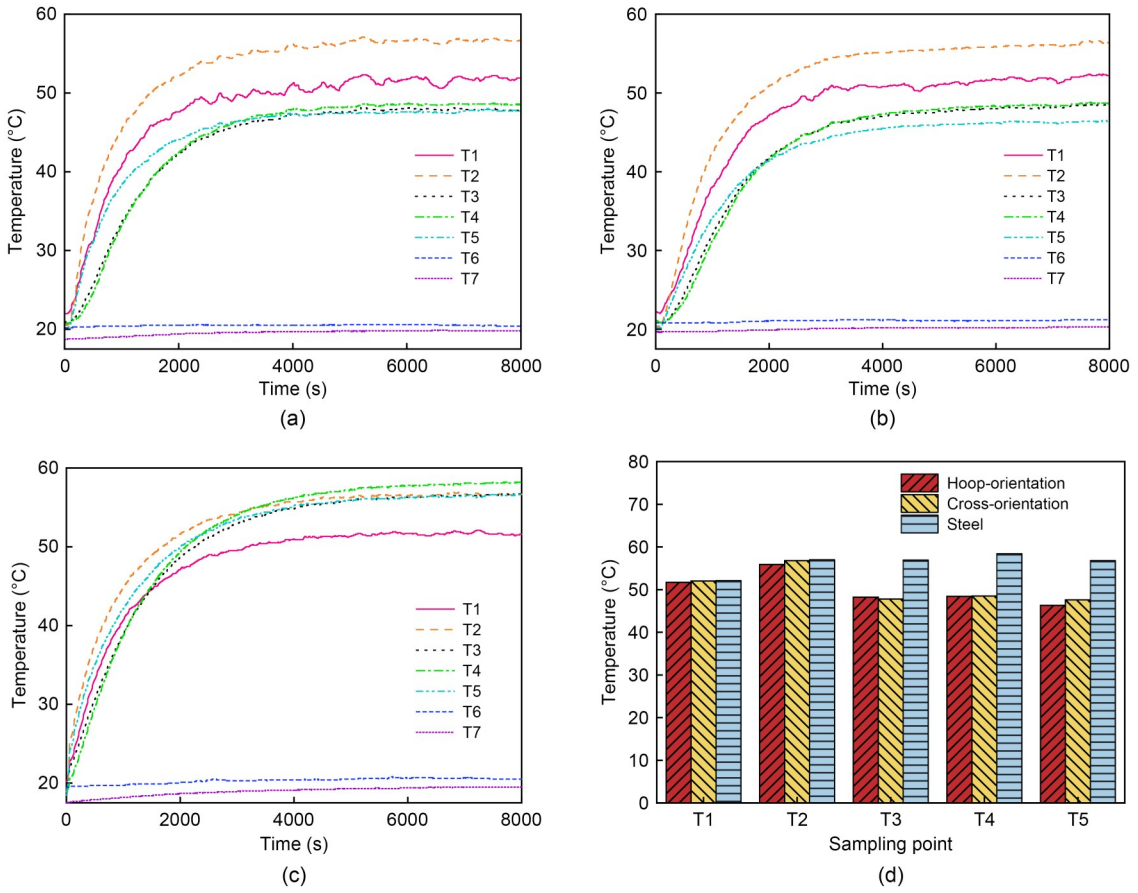

Fig. 13 Surface temperatures of (a) a hybrid shaft with cross-orientation CF/PEEK, (b) a hybrid shaft with hoop-orientation CF/PEEK, and (c) a steel shaft, and (d) a comparison of temperatures of five points

hybrid shafts was the highest, while on the steel shaft it was a relatively low temperature. The heat dissipation in the area between the two bearing areas was limited due to the insulation plate reducing convection in the centre channel of all three shafts, resulting in a large temperature rise at points T3, T4, and T5 on the steel shaft. Overall, the decrease in surface temperature at the CF/PEEK-covered area ranged from 14.7% to 18.2%. Precisely, at T3, T4, and T5, the temperature decreased from 58.4, 56.9, and 56.8 ℃ for the steel shaft to 47.8, 48.5, 47.6 ℃ for the steel–CF/PEEK hybrid shaft with cross-orientation and 48.2, 48.4, and 46.3 ℃ for the steel–CF/PEEK hybrid shaft with hoop-orientation, respectively. In addition to the effect of convection heat transfer, CF/PEEK prepreg tapes not only have a larger specific heat capacity but also have an emissivity of 0.71, while the emissivity of S45C steel at room temperature is about 0.13, resulting in a decrease in surface temperature.

Although the temperature difference between the corresponding temperature measurement points was not significant, temperatures at three measurement points on the steel–CF/PEEK hybrid shaft with a cross-orientation arrangement were lower than those of the steel–CF/PEEK hybrid shaft with a hoop-orientation arrangement. The thermal conductivity of CFs along the fibre direction is about three times that of steel. When the cross-orientation arrangement was applied, the entire CF/PEEK area had higher thermal conductivity along the axis direction, resulting in a more uniform temperature distribution on the outside surface of the CF/PEEK layer. Therefore, the high thermal conductivity of CF could be used to transfer the heat at the contact interface between the shaft and bearings to the outside surface of the CF/PEEK-covered area in contact with air for rapid heat dissipation. The uniform distribution of surface temperature also indicates that the temperature distribution inside the CF layer is relatively uniform along the axial direction. This will help improve the design and theory of hybrid shafts in future work.

The axial and radial thermal deformations of the two hybrid shafts and the steel shaft were measured (Fig. 14). Compared with the steel shaft, the thermal displacement in the axial direction of the hybrid shaft with cross-orientation arrangement was decreased by about 11.5%, from 279 to 247 μm, while the axial displacement of the hybrid shaft with hoop-orientation

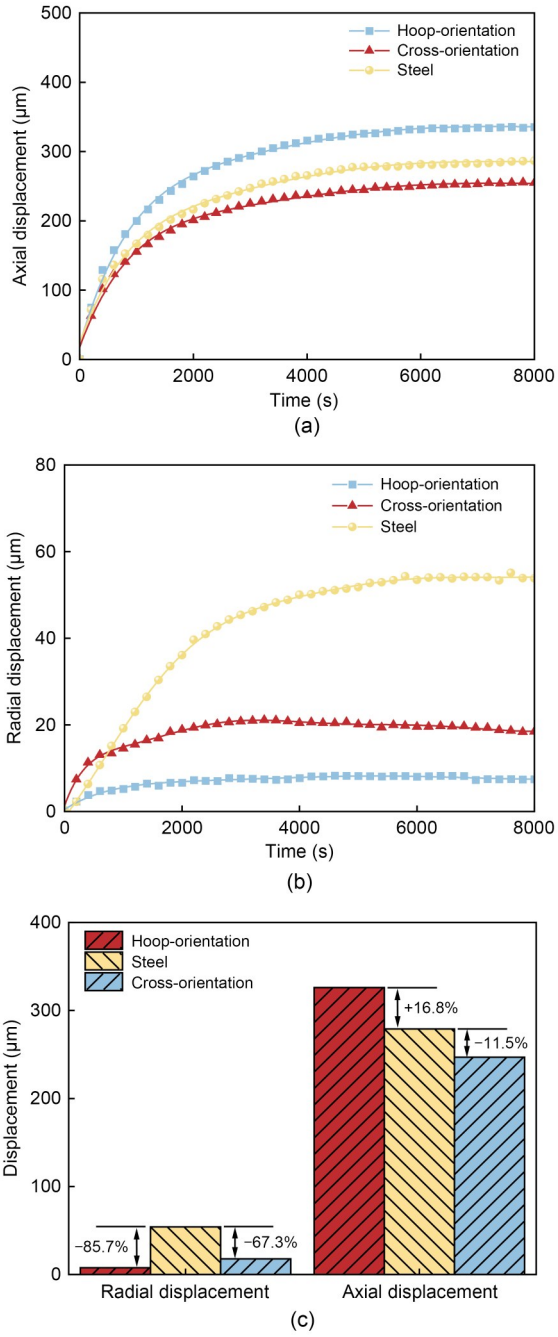

Fig. 14 Displacements of the three shafts: (a) axial displacement; (b) radial displacement; (c) comparison of the displacements

arrangement was increased by about 16.8%, to 326 μm (Fig. 14a). This indicates that a larger proportion of CFs arranged along the axis direction leads to a more significant impact on restricting axial thermal deformation of the steel–CF/PEEK hybrid shaft. On the other hand, high-modulus CF, as well as the characteristics of thermal shrinkage in the fibre direction, restricted

the deformation in the radial direction. Therefore, the thermal expansion of the hybrid shaft with the hoop-orientation arrangement in the axial direction was more pronounced.

For radial displacement measurement, the experimental conditions were identical to those used for the measurement of axial deformation. According to the results, the radial deformation of the S45C steel shaft was 54.1 μm while the radial deformation of the steel–CF/PEEK hybrid shaft was 7.7 μm with hoop-orientation and 17.7 μm with cross-orientation arrangement, namely an 85.7% and 67.3% reduction, respectively (Fig. 14b). This indicates that the hoop-orientation method has a remarkable effect on suppressing radial deformation. As for the steel–CF/PEEK hybrid shaft with cross-orientation, although only one layer of CF/PEEK prepreg tape was arranged at a 90° angle to the axis, it still had a restraining effect on radial deformation.

4 Conclusions

A novel steel–CF/PEEK hybrid shaft was proposed and manufactured using a laser-assisted in-situ consolidation process. Firstly, the optimal process parameters were investigated through SBS tests. The highest SBS strength of 80.7 MPa was acquired at a process temperature of 500 ℃ and a placement speed of 100 mm/s. In addition, two failure modes of interlayer cracks and inelastic deformation for SBS samples were observed, and the inelastic deformation was associated with a higher SBS strength. Furthermore, crack propagation was analyzed using DIC, and a maximum crack of 0.1046 mm was observed. Meanwhile, the internal defects and porosities of two samples with different process parameters were measured through X-ray tomography. A porosity of 0.23% with clear interlayer resin enrichment areas was found within the sample manufactured at 400 ℃ with a 75 mm/s placement speed, while a porosity of only 0.01% without a resin enrichment area was acquired when the sample was manufactured with optimal parameters of 500 ℃ and 100 mm/s. Finally, two hybrid shafts, with different fibre arrangements, were manufactured with the optimal process parameters. Their surface temperature distributions and thermal displacements were measured and compared with those of the steel shaft. The surface temperature decreased by 14.7%–18.2% at the CF/PEEK-covered area compared with the steel shaft. An 11.5% decrease in axial deformation for the steel–CF/PEEK hybrid shaft with cross-orientation was achieved, compared to the steel shaft. Moreover, for the steel–CF/PEEK hybrid shaft, the radial displacement decreased by 67.3% with cross-orientation and by 85.7% with hoop-orientation. Therefore, the proposed steel–CF/PEEK hybrid shaft, together with the manufacturing process, shows great potential for suppressing shaft thermal deformation.

Acknowledgments

This work is supported by the National Nature Science Foundation of China (No. 52175440), the Aeronautics Science Foundation of China (No. 2023Z049076001), the Science and Technology Innovation Fund of Shanghai Aerospace (No. SAST2022-058), the Open Fund of State Key Laboratory of Mechanical Transmissions (No. SKLMT-MSKFKT-202202), the Key R&D Program of Zhejiang Province (No. 2023C01058), and the Experimental Technique Project of Zhejiang University (No. SYBJS202302), China.

Author contributions

Zequan DING: methodology, visualization, investigation, and writing–original draft. Congcong LUAN, Xinhua YAO, and Jianzhong FU: conceptualization, supervision, project administration, funding acquisition, resources, and writing–review & editing. Yuyang JI, Chengcheng NIU, and Ningguo DONG: data curation, visualization, and investigation. Lingyu CHENG, Kai ZHAO, and Zhibin RUAN: visualization.

Conflict of interest

Zequan DING, Congcong LUAN, Xinhua YAO, Lingyu CHENG, Yuyang JI, Chengcheng NIU, Ningguo DONG, Kai ZHAO, Zhibin RUAN, and Jianzhong FU declare that they have no conflict of interest.

References

ASTM (American Society for Testing and Materials), 2024. Standard Test Method for Short-Beam Strength of Polymer Matrix Composite Materials and Their Laminates, ASTM D2344/D2344M-24. ASTM International, West Conshohocken, USA.

Bao L, Xu YL, Zhou Q, et al., 2023. Thermal error modeling of numerical control machine based on beetle antennae search back-propagation neural networks. *International Journal of Computational Intelligence Systems*, 16(1):84. https://doi.org/10.1007/s44196-023-00263-0

Cebe P, Chung SY, Hong SD, 1987. Effect of thermal history on mechanical properties of polyetheretherketone below the glass transition temperature. *Journal of Applied Polymer Science*, 33(2):487-503. https://doi.org/10.1002/app.1987.070330217

Çelik O, Peeters D, Dransfeld C, et al., 2020. Intimate contact development during laser assisted fiber placement: microstructure and effect of process parameters. *Composites Part A: Applied Science and Manufacturing*, 134:105888. https://doi.org/10.1016/j.compositesa.2020.105888

Çelik O, Hosseini SMA, Baran I, et al., 2021. The influence of inter-laminar thermal contact resistance on the cooling of material during laser assisted fiber placement. *Composites Part A: Applied Science and Manufacturing*, 145: 106367. https://doi.org/10.1016/j.compositesa.2021.106367

Cirino M, Pipes RB, Friedrich K, 1987. The abrasive wear behaviour of continuous fibre polymer composites. *Journal of Materials Science*, 22(7):2481-2492. https://doi.org/10.1007/BF01082134

Comer AJ, Ray D, Obande WO, et al., 2015. Mechanical characterisation of carbon fibre–PEEK manufactured by laser-assisted automated-tape-placement and autoclave. *Composites Part A: Applied Science and Manufacturing*, 69: 10-20. https://doi.org/10.1016/j.compositesa.2014.10.003

Ding JT, Xu L, Ma Z, et al., 2016. The lightweight structure design of a CFRP mirror. Proceedings of the 8th International Symposium on Advanced Optical Manufacturing and Testing Technologies: Advanced Optical Manufacturing Technologies, article 96831X. https://doi.org/10.1117/12.2243440

Donough MJ, Shafaq, John NA, et al., 2022. Process modelling of in-situ consolidated thermoplastic composite by automated fibre placement–a review. *Composites Part A: Applied Science and Manufacturing*, 163:107179. https://doi.org/10.1016/j.compositesa.2022.107179

Fan KG, Xu RF, Wang RD, et al., 2022. Thermoelectric-based cooling system for high-speed motorized spindle II: optimization and validation strategy. *The International Journal of Advanced Manufacturing Technology*, 119(9-10): 6521-6533. https://doi.org/10.1007/s00170-022-08709-z

Ge ZJ, Ding XH, 2018. Design of thermal error control system for high-speed motorized spindle based on thermal contraction of CFRP. *International Journal of Machine Tools and Manufacture*, 125:99-111. https://doi.org/10.1016/j.ijmachtools.2017.11.002

Grove S, 1993. Thermoplastic aromatic polymer composites: a study of the structure, processing and properties of carbon fibre-reinforced polyetheretherketone and related materials. *Composites Manufacturing*, 4(1):59. https://doi.org/10.1016/0956-7143(93)90018-4

Guo ZC, He JJ, Gao RX, et al., 2024. Molding of polyether ether ketone (PEEK) and its composites: a review. *Journal of Zhejiang University-SCIENCE A*, 25(10):788-823. https://doi.org/10.1631/jzus.A2400004

Ji SJ, Yu HJ, Zhao J, et al., 2015. Comparison of mechanical property and machinability for polyetheretherketone and glass fiber-reinforced polyetheretherketone. *Advances in Mechanical Engineering*, 7(4). https://doi.org/10.1177/1687814015578357

Ji YY, Luan CC, Yao XH, et al., 2023. Mechanism and behavior of laser irradiation on carbon fiber reinforced polyetheretherketone (CF/PEEK) during the laser-assisted in-situ consolidation additive manufacturing process. *Additive Manufacturing*, 74:103713. https://doi.org/10.1016/j.addma.2023.103713

Jiang W, Chen C, Chen ZK, et al., 2023. Effect of crystallinity on optical properties of PEEK prepreg tapes for laser-assisted automated fiber placement. *Composites Communications*, 38:101490. https://doi.org/10.1016/j.coco.2022.101490

Lei MH, Gao F, Li Y, et al., 2022. Feedback control–based active cooling with pre-estimated reliability for stabilizing the thermal error of a precision mechanical spindle. *The International Journal of Advanced Manufacturing Technology*, 121(3-4):2023-2040. https://doi.org/10.1007/s00170-022-09471-y

Levy A, Heider D, Tierney J, et al., 2014. Inter-layer thermal contact resistance evolution with the degree of intimate contact in the processing of thermoplastic composite laminates. *Journal of Composite Materials*, 48(4):491-503. https://doi.org/10.1177/0021998313476318

Li MY, Ma C, Zeng S, et al., 2023a. Cooling water jacket design of motorized spindle system using multi-objective topology optimization. *Applied Thermal Engineering*, 224: 120112. https://doi.org/10.1016/j.applthermaleng.2023.120112

Li MY, Ma C, Liu JL, 2023b. Topology optimization design of cooling water jacket structure for highspeed spindle-bearing system. *Journal of Manufacturing Processes*, 102: 1-22. https://doi.org/10.1016/j.jmapro.2023.07.034

Li Y, Bai YM, Hou ZY, et al., 2023a. Thermal error modeling and compensation of spindle based on gate recurrent unit network. *The International Journal of Advanced Manufacturing Technology*, 128(11):5519-5528. https://doi.org/10.1007/s00170-023-12276-2

Li Y, Liu ZT, Li L, et al., 2023b. Topology structural design and thermal characteristics analysis of high-efficiency heat conductive path for the spindle system. *Processes*, 11(9):2650. https://doi.org/10.3390/pr11092650

Li ZL, Wang BD, Zhu WM, et al., 2023. Design and thermal characteristic analysis of motorized spindle cooling water jacket. *The International Journal of Advanced Manufacturing Technology*, 128(7-8):3331-3342. https://doi.org/10.1007/s00170-023-12162-x

Lu QB, Zhu D, Wang M, et al., 2023. Digital twin-driven thermal error prediction for CNC machine tool spindle. *Lubricants*, 11(5):219. https://doi.org/10.3390/lubricants11050219

Mayr J, Jedrzejewski J, Uhlmann E, et al., 2012. Thermal issues in machine tools. *CIRP Annals*, 61(2):771-791. https://doi.org/10.1016/j.cirp.2012.05.008

Miao QY, Dai ZH, Ma GY, et al., 2021. Effect of consolidation force on interlaminar shear strength of CF/PEEK laminates manufactured by laser-assisted forming. *Composite Structures*, 266:113779. https://doi.org/10.1016/j.compstruct.2021.113779

Moddeman WE, Bowling WC, Tibbitts EE, et al., 1986. Thermal

stability and compatibility of polyetheretherketone (PEEK) with an oxidizer and pyrotechnic blend. *Polymer Engineering & Science*, 26(21):1469-1477. https://doi.org/10.1002/pen.760262102

Namba Y, 2001. Breakage of glass-ceramic spindle of zero-thermal-expansion. *The Proceedings of the Manufacturing & Machine Tool Conference*, 3:167-168 (in Japanese). https://doi.org/10.1299/jsmemmt.2001.3.167

Niu CC, Shen HY, Luan CC, et al., 2024. Optimization and assessment of CF/PEEK-PEEK composite shell manufactured by the laser-assisted in situ consolidation integrated with material extrusion process. *Journal of Manufacturing Process*, 119:452-462. https://doi.org/10.1016/j.jmapro.2024.03.100

Pratte J, 2012. Polyetheretherketone (PEEK) composites: an update on processing-morphology-property relationships. *In*: Nicolais L (Ed.), Wiley Encyclopedia of Composites. John Wiley & Sons, Inc., USA. https://doi.org/10.1002/9781118097298.weoc175

Song L, Liu K, Zhao D, et al., 2023. The spindle axial time-varying thermal error compensation method for horizontal boring and milling machine tool based on edge computing. *The International Journal of Advanced Manufacturing Technology*, 128(5-6):2631-2638. https://doi.org/10.1007/s00170-023-11927-8

Stokes-Griffin CM, Compston P, 2015. The effect of processing temperature and placement rate on the short beam strength of carbon fibre–PEEK manufactured using a laser tape placement process. *Composites Part A: Applied Science and Manufacturing*, 78:274-283. https://doi.org/10.1016/j.compositesa.2015.08.008

Stokes-Griffin CM, Compston P, 2016. Investigation of sub-melt temperature bonding of carbon-fibre/PEEK in an automated laser tape placement process. *Composites Part A: Applied Science and Manufacturing*, 84:17-25. https://doi.org/10.1016/j.compositesa.2015.12.019

Vermeulen JPMB, Rosielle PCJN, Schellekens PHJ, 2000. An advanced ceramic optical diamond turning machine design and prototype development. *CIRP Annals*, 49(1):407-410. https://doi.org/10.1016/S0007-8506(07)62976-X

Xia CH, Fu JZ, Lai JT, et al., 2015. Conjugate heat transfer in fractal tree-like channels network heat sink for high-speed motorized spindle cooling. *Applied Thermal Engineering*, 90:1032-1042. https://doi.org/10.1016/j.applthermaleng.2015.07.024

Xu L, Xie YJ, Ding JT, et al., 2016. The design and optimization of carbon fiber laminates based on thermal stability and bending rigidity. *Fiber Reinforced Plastics/Composites*, (2): 57-61 (in Chinese).

Zheng DX, Chen WF, 2022. Effect of a cooling unit on high-speed motorized spindle temperature with a scaling factor. *The International Journal of Advanced Manufacturing Technology*, 120(3-4):2559-2572. https://doi.org/10.1007/s00170-022-08958-y